J Mater Sci: Mater Electron (2016) 27:834–842
DOI 10.1007/s10854-015-3824-3

Nanocrystalline barium stannate: facile morphology-controlled preparation, characterization and investigation of optical and photocatalytic properties

Saeed Moshtaghi[1] · Sahar Zinatloo-Ajabshir[1] · Masoud Salavati-Niasari[1]

Received: 25 July 2015 / Accepted: 2 October 2015 / Published online: 7 October 2015

Abstract Pure cubic nanocrystalline barium stannate was synthesized by new simple coprecipitation strategies that employed tin (II) chloride and [bis(salicylaldehydato) barium (II)] as tin and barium sources in presence of tetramethylethylenediamine (TMED) as a novel precipitating agent. This work is the first successful attempt for the preparation of nanostructured barium stannate by utilizing TMED via a facile coprecipitation way in presence of tin (II) chloride and [bis(salicylaldehydato) barium (II)]. The structural, optical and morphological characteristics of the as-prepared nanostructured barium stannate were studied by UV–vis diffuse reflectance spectroscopy, transmission electron microscopy, X-ray diffraction, scanning electron microscopy (SEM), Fourier transform infrared spectroscopy and energy dispersive X-ray microanalysis (EDX). According to the SEM results, it was found that shape and size of the barium stannate can be dramatically controlled by setting critical preparation factors such as the barium source, precipitating agent type, reaction pH, surfactant type and dosage of surfactant. The photocatalytic characteristics of as-obtained nanocrystalline barium stannate were also examined by degradation of erythrosine dye as water contaminant.

✉ Masoud Salavati-Niasari
salavati@kashanu.ac.ir

[1] Institute of Nano Science and Nano Technology, University of Kashan, P. O. Box 87317-51167, Kashan, Islamic Republic of Iran

1 Introduction

Barium stannate belongs to the family of the alkaline earth stannates. Since barium stannate has remarkable and excellent dielectric, photovoltaic, optical and electrical characteristics [1–3], it has become one of the most significant and considerable materials for catalyst support, protective coating, sensor, capacitors, ceramic, solar cell and photocatalyst [1, 4–9]. Barium stannate has perovskite structure and cubic crystal phase [10]. So far, reverse micelle, solid state, coprecipitation, combustion and sol–gel approach [11–15] have been reported to synthesize barium stannate. Since shape, size and size distribution have key and considerable impact on the characteristics and applications of the nanomaterials, several procedures have been reporting on particle size and shape controlled preparation of nanomaterials [16–24].

Herein, pure cubic nanocrystalline barium stannate is prepared via a new facile coprecipitation way by employing tin (II) chloride and [bis(salicylaldehydato) barium (II)] in presence of tetramethylethylenediamine (TMED) as a new precipitating agent. The coprecipitation approach is well known as a reliable and effective route for particle size and shape controlled preparation of many nanomaterials. To our knowledge, it is the first time that TMED is employed as a precipitating agent in presence of tin (II) chloride and [bis(salicylaldehydato) barium (II)] for the preparation of nanocrystalline barium stannate and the influences of different synthesis factors on the shape and particle size of the barium stannate through a facile coprecipitation way are examined. Furthermore, the photocatalytic characteristics of the as-prepared nanocrystalline barium stannate were investigated by photocatalytic degradation of erythrosine dye as model water pollutant under UV light illumination.

2 Materials and methods

2.1 Materials and characterization

Tin(II) chloride, barium nitrate, TMED, methanol, ethylenediamine (en), cetyltrimethyl ammonium bromide (CTAB), salicylaldehyde ($C_7H_6O_2$), liquor ammonia solution containing 25 % ammonia and sodium dodecyl sulphate (SDS) with analytical grade were bought from Merck and were applied without additional purification. SEM images of barium stannate samples were visualized by a Hitachi S-4160 field emission scanning electron microscope (FESEM). Transmission electron microscope (TEM) images of as-synthesized nanocrystalline barium stannate were taken on a JEM-2100 with an accelerating voltage of 200 kV. Fourier transform infrared spectra of bis(salicylaldehydato) barium (II)] and as-prepared nanocrystalline barium stannate were obtained on a Shimadzu Varian 4300 spectrophotometer in KBr pellets in the 400–4000 cm^{-1} range. The UV–vis diffuse reflectance spectrum of the as-prepared nanocrystalline barium stannate was obtained on a UV–vis spectrophotometer (Shimadzu, UV-2550, Japan). The EDS analysis was carried out by a Philips XL30 microscope. Powder X-ray diffraction (XRD) pattern of the as-obtained nanocrystalline barium stannate was recorded by applying a diffractometer of Philips Company with X'PertPromonochromatized Cu Kα radiation ($\lambda = 1.54$ Å).

2.2 Preparation of [bis(salicylaldehydato) barium (II)]

To prepare [bis(salicylaldehydato) barium (II)], 8 mmol of $C_7H_6O_2$ was dissolved in 80 ml of methanol and then was drop-wise added to 80 ml solution containing 4 mmol of barium nitrate under magnetic stirring. The mixture was refluxed for 3 h.

2.3 Preparation of nanocrystalline barium stannate

Nanocrystalline barium stannate was prepared by new facile coprecipitation method. To prepare barium stannate, in a typical procedure, 0.07 g of tin(II) chloride was dissolved in hot distilled water (60 °C) and then was added drop-wise to 20 ml hot solution (60 °C) containing 0.125 g of [bis(salicylaldehydato) barium (II)] under magnetic stirring. The pH of the obtained solution was adjusted to 13 by adding NH_3 solution drop-wise and resultant solution was heated at 60 °C for 1 h under constant magnetic stirring. The final product was air-dried and calcined at 700 °C for 4 h (sample no. 1). Scheme 1 exhibits the schematic diagram of the preparation of the nanocrystalline barium stannate. For studying the effect of the surfactant, a certain dosage of the surfactant was dissolved in 2 ml distilled water and added after mixing [bis(salicylaldehydato) barium (II)] and tin(II) chloride solutions. The effect of the barium source, precipitating agent type, reaction pH, surfactant type and dosage of surfactant on the morphology and particle size of the barium stannate were also examined (Table 1).

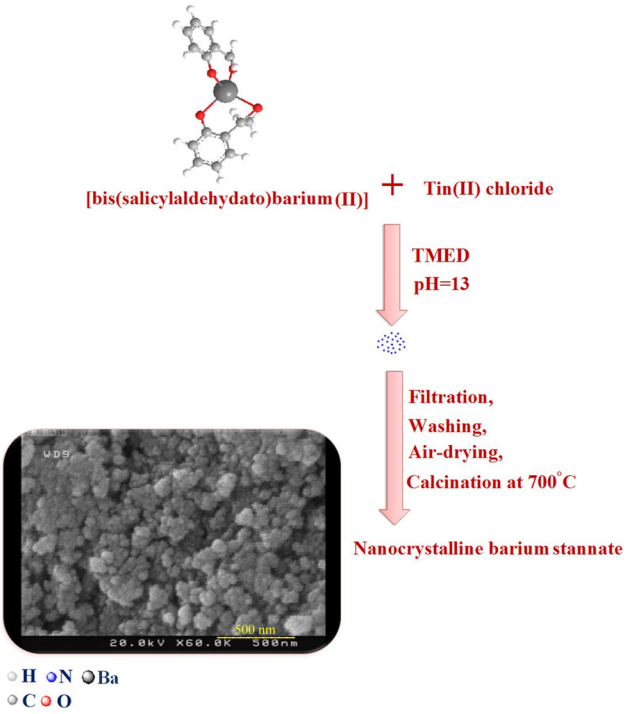

Scheme 1 Schematic diagram of the preparation of the nanocrystalline barium stannate

2.4 Photocatalytic measurements

The photocatalytic characteristics of the as-synthesized nanocrystalline barium stannate were examined by utilizing of the anionic dye (erythrosine) solution. The reaction solution including the 0.001 g of the erythrosine and 0.004 g of the as-prepared barium stannate in the quartz reactor was applied to examine the photocatalytic characteristics. After aerating for 30 min, the mixture was subjected to the irradiation of the UV light from the 400 W mercury lamps. The anionic dye photodegradation percentage was calculated as follow:

$$\text{D.P.}(t) = \frac{A_0 - A_t}{A_0} \times 100 \quad (1)$$

where A_t and A_0 are the absorbance quantity of anionic dye solution at t and 0 min by a UV–vis spectrometer, respectively.

Table 1 The preparation conditions of the barium stannate micro/nanostructures

Sample No.	Precipitating agent	Ba source	Reaction pH	Surfactant type	CTAB:Ba:Sn molar ratio	Figure of SEM images
1	NH_3	[bis(salicylaldehydato) barium (II)]	13	–	–	3a
2	en	[bis(salicylaldehydato) barium (II)]	13	–	–	3b
3	TMED	[bis(salicylaldehydato) barium (II)]	13	–	–	3c
4	TMED	[bis(salicylaldehydato) barium (II)]	11	–	–	4a
5	TMED	[bis(salicylaldehydato) barium (II)]	9	–	–	4b
6	TMED	[bis(salicylaldehydato) barium (II)]	13	SDS	1:1:1	5a
7	TMED	[bis(salicylaldehydato) barium (II)]	13	CTAB	1:1:1	5b
8	TMED	[bis(salicylaldehydato) barium (II)]	13	CTAB	0.5:1:1	6a
9	TMED	[bis(salicylaldehydato) barium (II)]	13	CTAB	2:1:1	6b
10[a]	TMED	$Ba(NO_3)_2$	13	–	–	7a

[a] Blank test

3 Results and discussion

In order to confirm the preparation of the [bis(salicylaldehydato) barium (II)] and barium stannate, Fourier transform infrared (FT-IR) analysis was performed. Figure 1a and b exhibits the infrared spectra of the [bis(salicylaldehydato) barium (II)] and as-prepared nanocrystalline barium stannate (sample no. 3), respectively. The bands appear at 1523 and 1636 cm^{-1} in Fig. 1a are attributable to the C–O stretching vibrations and the band appears at 1433 cm^{-1} is attributable to the C–C stretching vibration of the $C_7H_6O_2$ compound. In the FT-IR spectrum of the free $C_7H_6O_2$ compound, the C–O stretching vibrations and C–C stretching vibration appear at 1680 and 1660 cm^{-1} as well as at 1490 cm^{-1}, respectively. These vibrations shifted to lower regions owing to [bis(salicylaldehydato) barium (II)] preparation [25]. In the FT-IR spectrum of the [bis(salicylaldehydato) barium (II)], the absorption peak located at 3307 cm^{-1} can be related to the stretching vibrations of the surface adsorbed water molecules. In Fig. 1a, absorption peak at 467 cm^{-1} can be related to Ba–O band, there is no peak around this point in $C_7H_6O_2$ compound. The absorption peak appear at 3426 cm^{-1} in Fig. 1b is attributable to the ν(OH) stretching vibration of physisorbed water molecules [22]. The characteristic band of the barium stannate appears at 646 cm^{-1} [26] (Fig. 1b).

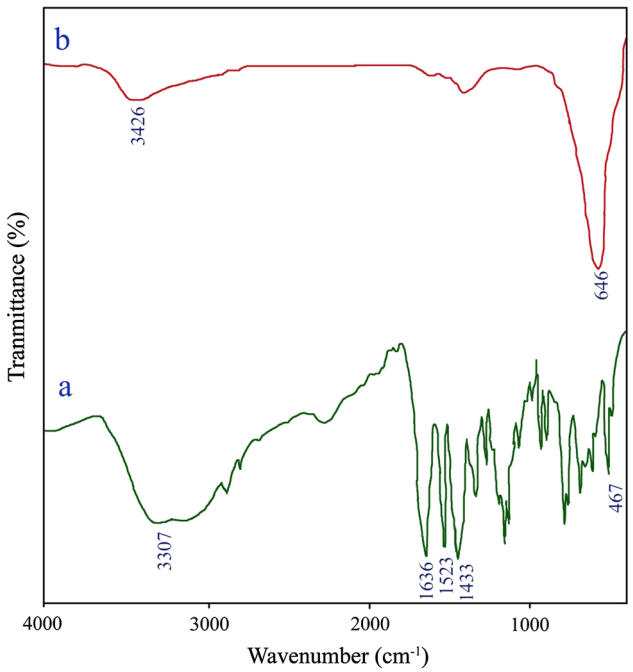

Fig. 1 FT-IR spectra of [bis(salicylaldehydato) barium (II)] (*a*) and nanocrystalline barium stannate (sample no. 3) (*b*)

To examine the chemical composition of the as-obtained nanocrystalline barium stannate (sample no. 3), the EDS analysis was carried out. As illustrated in Fig. 2a, the sample no. 3 is composed of Ba, Sn and O elements.

In order to characterize the crystalline structure of the as-prepared barium stannate (sample no. 3), XRD pattern was taken and exhibited in Fig. 2b. All of the diffraction peaks illustrated in this XRD pattern are well-matched to pure cubic $BaSnO_3$ (space group Pm-3m, JCPDS card 15-0780). No impurities can be found in Fig. 2b, demonstrating that a pure barium stannate has been synthesized. The crystallite size of the nanocrystalline barium stannate (sample no. 3) determined by the Scherrer equation [17] is 21 nm.

To examine the influence of the critical preparation factors such as the barium source, precipitating agent type, reaction pH, surfactant type and dosage of surfactant on the morphological properties of the barium stannate SEM analysis was applied. To study the influence of the precipitating agent type on the shape and size of the barium stannate, the three different precipitating agent including ammonia, en and TMED were employed (sample nos.

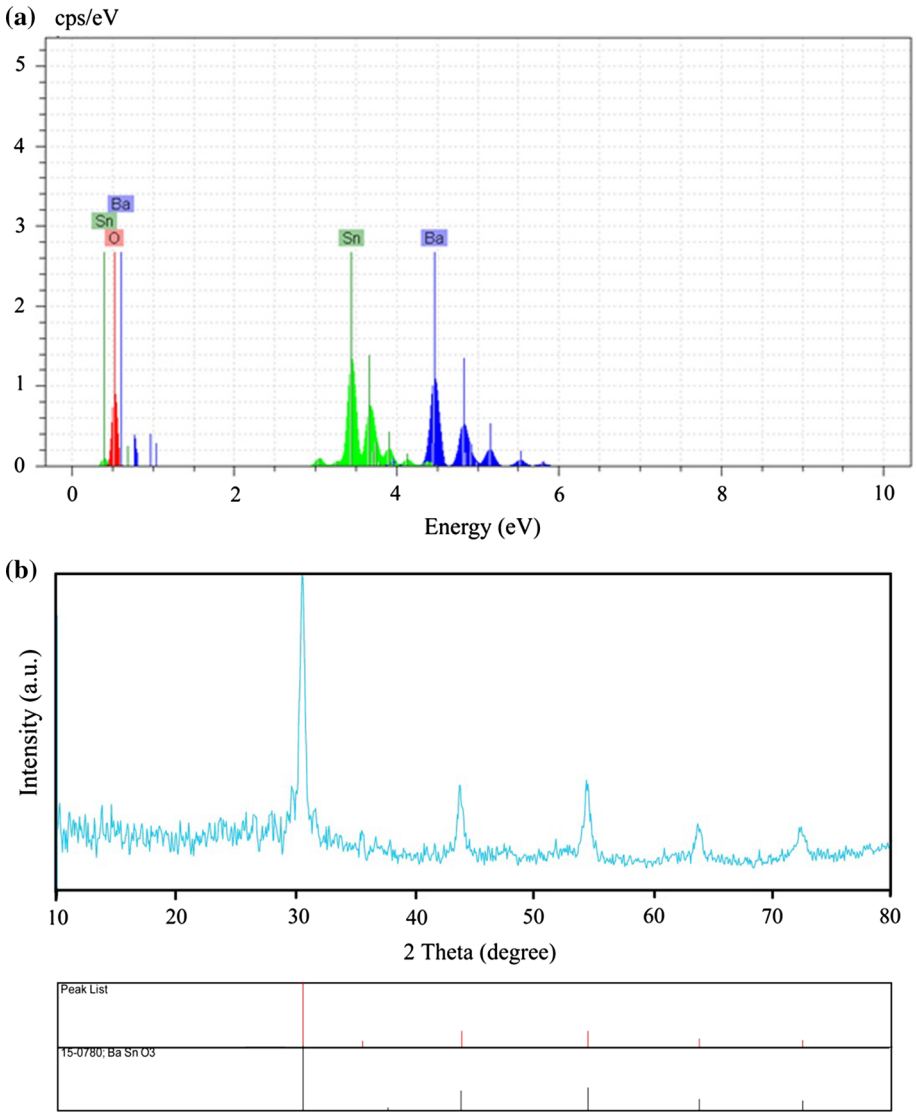

Fig. 2 EDS (**a**) and XRD (**b**) patterns of the nanocrystalline barium stannate (sample no. 3)

1–3). Figure 3a–c exhibits SEM images of sample nos. 1–3 formed in the presence of the ammonia, en and TMED, respectively. As illustrated in Fig. 3a–c, by employing ammonia, en and TMED, the coalesced particles/bulk structures, irregular micro/nanostructures and nanoparticles with uniform spherical shape are formed, respectively. It can be observed that the size of the particles becomes smaller and the amount of uniform barium stannate nanostructures increases by changing the precipitating agent type from ammonia to TMED (Fig. 3a–c). It seems that when TMED with highest steric hindrance influence (Scheme 2) employs, the nucleation to be happened rather than the particle growth. TMED with high steric hindrance influence can act as capping agent and decreases the chance of collision between as-formed nanoparticles. According to the SEM results, TMED is the best precipitating agent that employed in our reaction conditions (Fig. 3c), and therefore other reactions were carried out by employing this precipitating agent.

To investigate the influence of the reaction pH on the shape and size of the barium stannate, the two samples were prepared at pH 9 and 11 (sample nos. 4 and 5), in the presence of the TMED (Fig. 4). It was observed that with decreasing reaction pH from 13 (Fig. 3c) to 11 (Fig. 4a) and 9 (Fig. 4b), the particles agglomeration and their size enhanced. It seems that when reaction pH decreases, TMED concentration decreases and therefore, the chance of the collision between formed nanoparticles increases. It can be deduced that 13 is the most desirable reaction pH for preparing the barium stannate nanoparticles with uniform spherical shape.

Furthermore, the influence of the surfactant type on the shape and size of the barium stannate was studied. SEM images of the barium stannate sample nos. 6 and 7 prepared

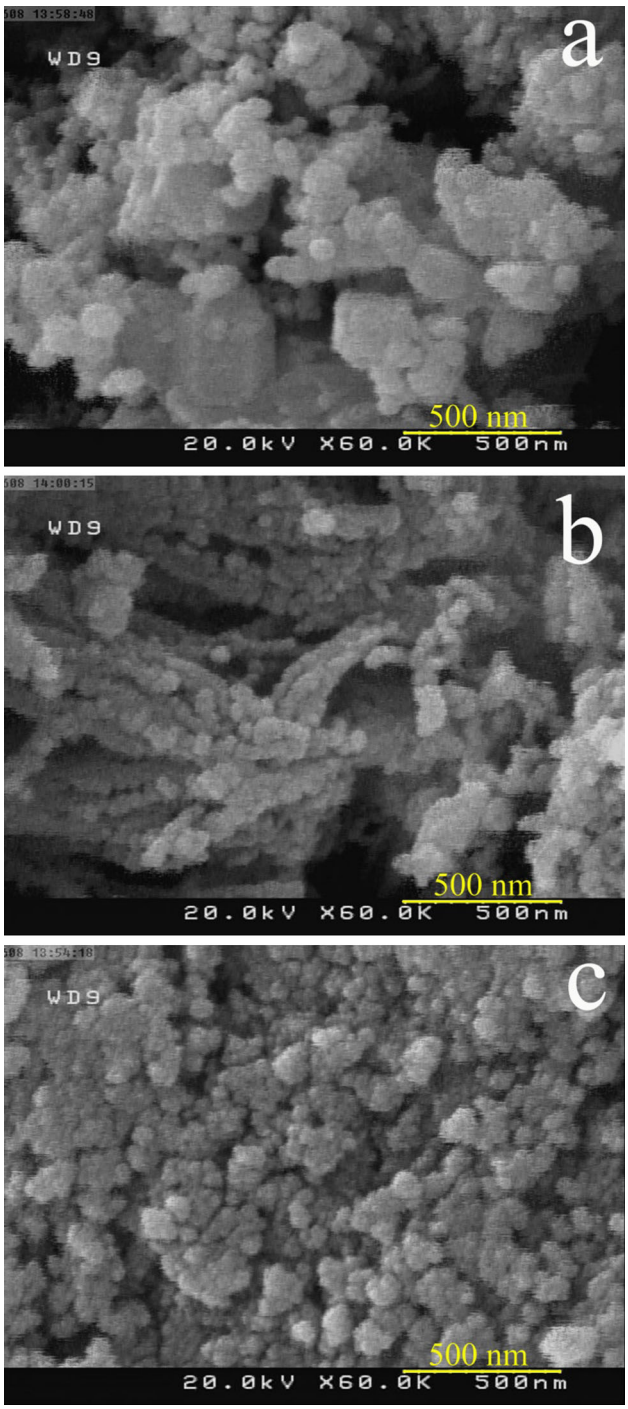

Fig. 3 SEM images of the samples prepared by **a** ammonia, **b** en and **c** TMED

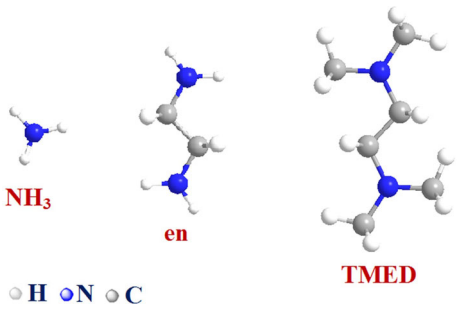

Scheme 2 Three different amines employed as precipitating agent

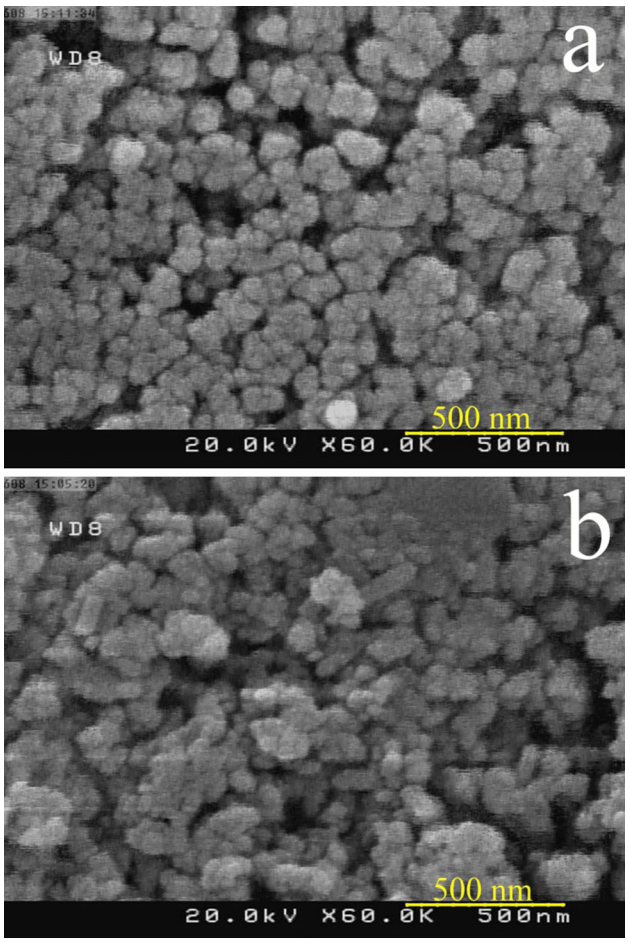

Fig. 4 SEM images of the samples synthesized at pH 11 (**a**) and 9 (**b**)

in the presence of the SDS and CTAB were taken and demonstrated in Fig. 5. By employing the SDS and CTAB, the high agglomerated particles/bulk structures and not uniform spherical nanostructures with large size are obtained, respectively (Fig. 5a, b). Between these employed surfactant types, CTAB with higher steric hindrance effect acts as better capping agent and causes not uniform spherical nanostructures with large size formed. To obtain nanostructures with uniform morphology in presence of the CTAB, CTAB dosage was changed. Figure 6a, b reveals the SEM images of the sample nos. 8 and 9 synthesized with CTAB:Ba:Sn molar ratio of 0.5:1:1 and 2:1:1, respectively. When 0.5:1:1 molar ratio was employed, the irregular micro/nanostructures of the barium stannate were prepared (Fig. 6a). By changing the molar ratio from 1:1:1 to 2:1:1, the particles agglomeration was

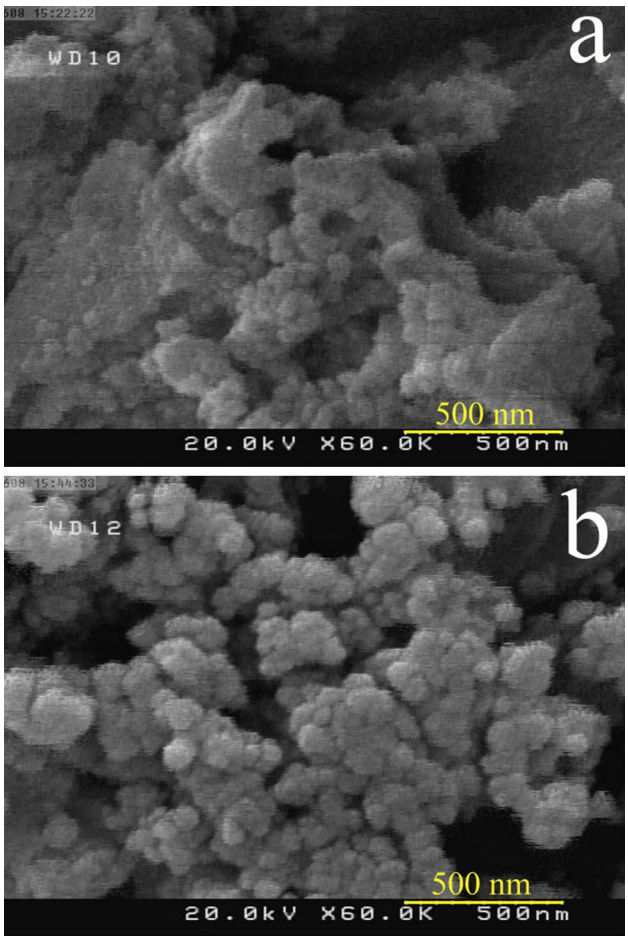

Fig. 5 SEM images of the samples prepared in the absence of **a** SDS and **b** CTAB

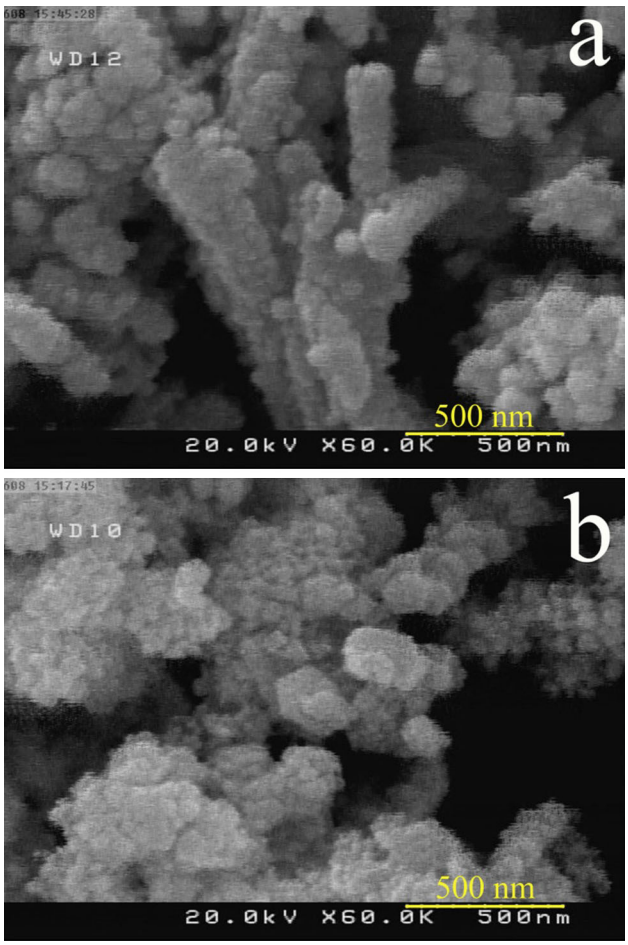

Fig. 6 SEM images of the samples synthesized with CTAB:Ba:Sn molar ratio of 0.5:1:1 (**a**) and 2:1:1 (**b**)

enhanced and, therefore not uniform nanostructures were formed (Fig. 6b). It seems that the large dosage of the CTAB causes the particles to be agglomerated. It is clear that the nanoparticles with uniform spherical shape are formed in absence of the surfactant (Fig. 3c) and employing the surfactant or changing the surfactant dosage does not lead to regular and uniform morphology. Maybe due to utilizing the [bis(salicylaldehydato) barium (II)], there is no requirement to employ any other surfactant type. It seems that the salicylaldehyde ligand with high steric hindrance influence in [bis(salicylaldehydato) barium (II)] can act as a capping agent and control the particle size and shape.

In continuation, the effect of the Ba source on the shape and size of the barium stannate was examined (Fig. 7a). SEM image of the barium stannate sample no. 10 as blank sample synthesized by utilizing barium nitrate and tin(II) chloride in the presence of the TMED at pH 13 was taken and demonstrated in Fig. 7a. It is noteworthy that bulk structures were prepared. The salicylaldehyde ligand with high steric hindrance influence in [bis(salicylaldehydato) barium (II)], can act as a capping agent. It is clear that the utilizing [bis(salicylaldehydato) barium (II)] as Ba source in presence of TMED brings about uniform spherical nanoparticles preparation (Fig. 3c). Thus, a special advantage of employing [bis(salicylaldehydato) barium (II)] is that it brings about nanocrystalline barium stannate formation.

To elucidate the detailed morphological characteristics of the as-prepared nanocrystalline barium stannate (sample no. 3) TEM images were taken. TEM images in Fig. 7b–d demonstrate that the nanoparticles are sintered together and their sizes are in the range 9–70 nm.

To examine the optical characteristics of the as-obtained nanocrystalline barium stannate (sample no. 3), UV–vis diffuse reflectance spectroscopy was employed. The UV–vis diffuse reflectance spectrum of the sample no. 3 is demonstrated in Fig. 8a. The absorption band at around 352 nm can be seen in the UV–vis diffuse reflectance spectrum. It is well known that the photocatalytic

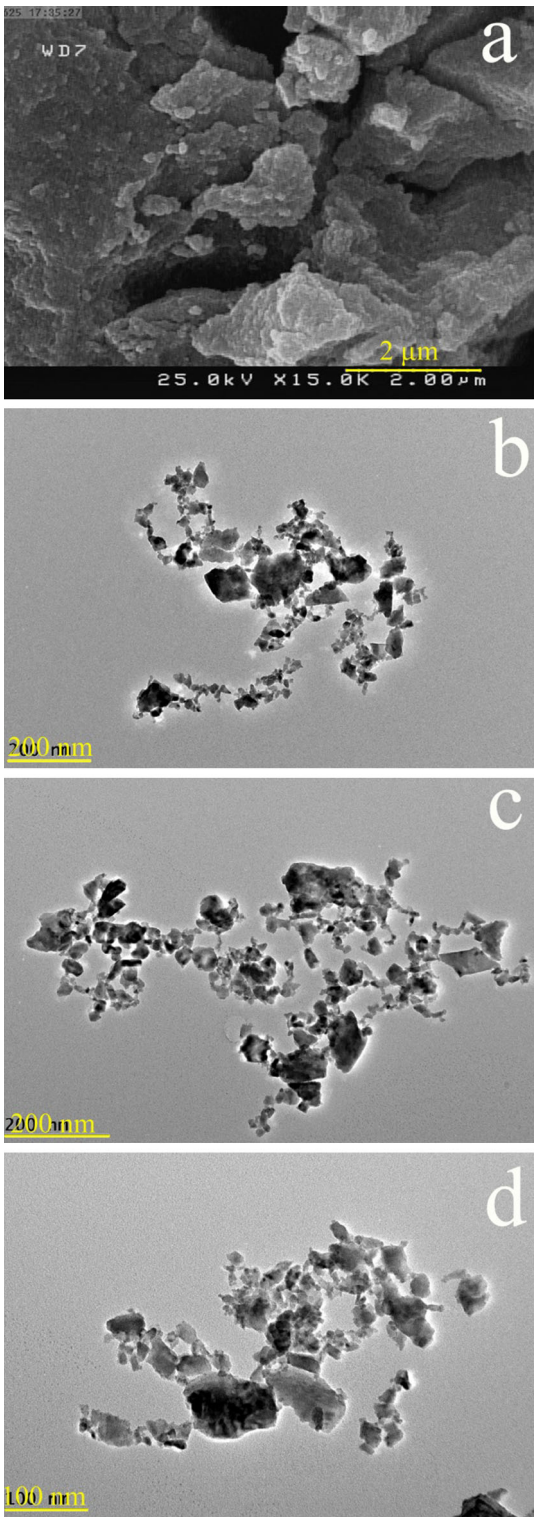

Fig. 7 SEM image of sample no. 10 obtained from barium nitrate and tin(II) chloride via coprecipitation procedure (**a**) and TEM images of sample no. 3 (**b** and **d**)

characteristics of the nanomaterials strongly depend on the band gap (Eg) factor. This key factor can be determined based on the UV–vis diffuse reflectance data utilizing

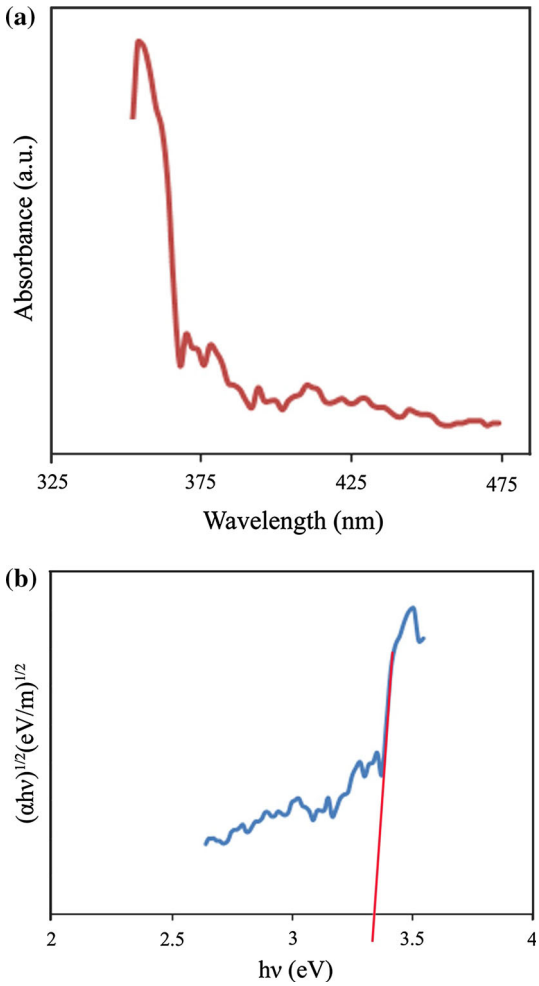

Fig. 8 UV-vis diffuse reflectance spectrum (**a**), plot to determine the band gap (**b**) of the nanocrystalline barium stannate (sample no. 3)

Tauc's equation [16]. The Eg of the nanocrystalline barium stannate as indirect semiconductor was determined by extrapolating the linear section of the plot of $(\alpha hv)^{1/2}$ against hv to the energy axis (Fig. 8b). The Eg quantity of the as-prepared nanocrystalline barium stannate estimated to be 3.3 eV. From the obtained Eg value, it is found that the as-obtained nanocrystalline barium stannate can be utilized as the photocatalyst.

In this work, photooxidation of the anionic dye (erythrosine) as water pollutant under UV light was employed to examine the photocatalytic characteristics of the as-prepared nanocrystalline barium stannate (sample no. 3). Figure 9a reveals the result of the photocatalytic test. No anionic dye (erythrosine) was practically broken down after 120 min in absence of the UV light or as-obtained nanocrystalline barium stannate. According to this obtained result, it was found that the contribution of self-degradation was insignificant. The possible mechanism of the degradation of erythrosine can be assumed as:

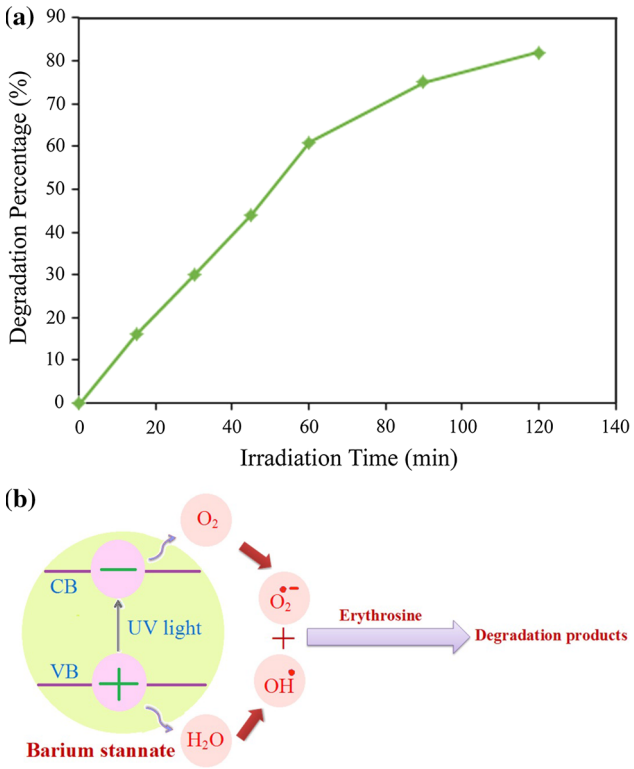

Fig. 9 Photocatalytic anionic dye (erythrosine) degradation of nanocrystalline barium stannate (sample no. 3) (**a**) and reaction mechanism of erythrosine photodegradation over nanocrystalline barium stannate under UV light irradiation

$$\text{Barium stannate} + h\nu \rightarrow \text{Barium stannate} * + e^- + h^+$$

$$h^+ + H_2O \rightarrow OH^{\cdot}$$

$$e^- + O_2 \rightarrow \cdot O_2^{-\cdot}$$

$$OH^{\cdot} + O_2^{-\cdot} + \text{Erythrosine} \rightarrow \text{Degradation products}$$

Based on the photocatalytic calculations by Eq. (1), the erythrosine degradation was about 82 % after 120 min illumination of UV light and the as-obtained nanocrystalline barium stannate illustrated high photocatalytic activity. In the heterogeneous photocatalytic processes, there are the diffusion, adsorption and reaction steps. It is generally accepted that photocatalytic activity depends mainly on the diffusion of reactants and products, and therefore the favorable distribution of the pore. It seems that the very well photocatalytic activity of the as-prepared nanocrystalline barium stannate can be due to the favorable distribution of the pore, high hydroxyl amount and high separation rate of the charge carriers [27, 31–36] (Fig. 9b).

In comparison to other studies, demonstrated in Table 2, our procedure is more facile, efficient, low-cost and friendly to the environment. In this research, we introduced a coprecipitation way to synthesize barium stannate with the aid of tin (II) chloride and [bis(salicylaldehydato) barium (II)] in presence of TMED as a novel precipitating agent and water as nontoxic solvent in milder conditions. The novelty of this investigation compared to other investigation is that for the preparation of the barium stannate, TMED as a novel precipitating agent in presence of tin (II) chloride and [bis(salicylaldehydato) barium (II)] was employed. TMED and salicylaldehyde ligand in [bis(salicylaldehydato) barium (II)] with high steric hindrance influence played capping agent role. Results of this study demonstrate that the usage of TMED in the presence of [bis(salicylaldehydato) barium (II)] led to the preparation of the barium stannate with high purity, uniform sphere-like morphology and small particle size.

4 Conclusions

This work presents a new facile coprecipitation way to prepare pure cubic nanocrystalline barium stannate with the aid of tetramethylethylenediamine (TMED) as a new precipitating agent in presence of tin (II) chloride and [bis(salicylaldehydato) barium (II)]. Utilizing of TMED both as a precipitating and capping agent in presence of bis(salicylaldehydato) barium (II)] is the novelty of this

Table 2 Characterization comparison of nanocrystalline barium stannate with other works

Method	Precursors	Size (nm)	Morphology	Ref.
Coprecipitation method.	$BaCl_2$, $SnCl_4$ and oxalic acid (needed calcining at 1050 °C)	0.2 μm	Relatively uniform grain-like powders	[28]
Sol–Gel route	$SnCl_4{\cdot}5H_2O$, isopropanol, anhydrous $BaCO_3$, anhydrous citric acid and ethylene glycol (needed calcining at 1000 °C)	40–60 nm	Not uniform nanoparticles	[29]
Coprecipitation method	$BaC1_2$, $SnCl_2$ and $H_2C_2O_4$ (needed calcining at 1000 °C)	0.08–0.14 μm	Not uniform nanoparticles	[30]
Thermal decomposition route	$BaCO_3$, $Sn(OH)_4$, (needed calcining at 1400 °C)	3–6 μm	Not uniform nanoparticles	[26]

investigation. By alteration of the barium source, precipitating agent type, reaction pH, surfactant type and dosage of surfactant, we could prepare nanocrystalline barium stannate with different particle sizes and shapes. When as-obtained barium stannate was employed as photocatalyst, the percentage of the erythrosine degradation was about 82 after 120 min irradiation of UV light. This result suggests as-synthesized barium stannate as interesting and favorable candidate for photocatalytic applications under UV light.

Acknowledgments The authors are grateful to University of Kashan for supporting this work by Grant No. (159271/520).

References

1. Z. Zhigang, Z. Gang, Ferroelectrics **101**, 43 (1990)
2. W. Zhang, J. Tang, J. Ye, J. Mater. Res. **22**, 1859 (2007)
3. H. Mizoguchi, H.W. Eng, P.M. Woodward, Inorg. Chem. **43**, 1667 (2004)
4. V.G. Wagner, H. Binder, Z. Anorg, Allg. Chem. **298**, 12 (1959)
5. P.H. Borse, J.S. Lee, H.G. Kim, J. Appl. Phys. **100**, 124915 (2006)
6. W. Wang, Sh Liang, K. Ding, J. Bi, J.C. Yu, P. Keung Wong, L. Wu, J. Mater. Sci. **49**, 1893 (2014)
7. S.S. Shin, J.S. Kim, J.H. Suk, K.D. Lee, D.W. Kim, J.H. Park, I.S. Cho, K.S. Hong, J.Y. Kim, ACS Nano **7**, 1027 (2013)
8. J. Cerda, J. Arbiol, G. Dezanneau, R. Díaz, J.R. Morante, Sensors Actuators B **84**, 21 (2002)
9. T. Huang, T. Nakamura, M. Itoh, Y. Inaguma, O. Ishiyama, J. Mater. Sci. **30**, 1556 (1995)
10. V. Vorgelegt, L. Wensheng, *Synthesis of Nanosized $BaSnO_3$ Powders*. Doctoral thesis in Engineering of Natural Sciences, (Faculty of Engineering, University of Saarlandes, Saarbrücken—Germany, 2002), pp. 1–2
11. S. Upadhyay, O. Parkash, D. Kumar, Mater. Lett. **49**, 251 (2001)
12. A.S. Deep, S. Vidya, P.C. Manu, S. Solomon, A. John, J.K. Thomas, J. Alloys Compd. **509**, 1830 (2011)
13. W. Lu, H. Schmidt, J. Sol-Gel. Sci. Technol. **42**, 55 (2007)
14. J. Ahmed, C.K. Blakely, S.R. Bruno, V.V. Poltavets, Mater. Res. Bull. **47**, 2282 (2012)
15. Y.H.O. Muñoz, M. Ponce, J. E. R. Páez Powder Technol. **279**, 86 (2015)
16. S. Mortazavi-Derazkola, S. Zinatloo-Ajabshir, M. Salavati-Niasari, Ceram. Int. **41**, 9593 (2015)
17. S. Zinatloo-Ajabshir, M. Salavati-Niasari, Int. J. Appl. Ceram. Technol. **11**, 654 (2014)
18. F. Beshkar, S. Zinatloo-Ajabshir, M. Salavati-Niasari, J. Mater. Sci.: Mater. Electron. **26**, 5043 (2015)
19. S. Zinatloo-Ajabshir, M. Salavati-Niasari, N. J. Chem. **39**, 3948 (2015)
20. M. Sabet, M. Salavati-Niasari, O. Amiri, Electrochim. Acta **117**, 504 (2014)
21. F. Beshkar, S. Zinatloo-Ajabshir, M. Salavati-Niasari, Chem. Eng. J. (2015). doi:10.1016/j.cej.2015.05.076
22. S. Zinatloo-Ajabshir, M. Salavati-Niasari, M. Hamadanian, RSC Adv. **5**, 33792 (2015)
23. S. Mortazavi-Derazkola, S. Zinatloo-Ajabshir, M. Salavati-Niasari, RSC Adv. **5**, 56666 (2015)
24. M. Shakouri-Arania, M. Salavati-Niasari, N. J. Chem. **38**, 1179 (2014)
25. M. Ghaed-Amini, M. Bazarganipour, M. Salavati-Niasari, J. Ind. Eng. Chem. **21**, 1089 (2015)
26. C.V.G. Reddy, S.V. Manorama, V.J. Rao, J. Mater. Sci.: Mater. Electron. **12**, 137 (2001)
27. J. Zhong, J. Li, F. Feng, Y. Lu, J. Zeng, W. Hu, Z. Tang, J. Mol. Catal. A: Chem. **357**, 101 (2012)
28. Y. Jung Song, S. Kim, J. Ind. Eng. Chem. **7**, 183 (2001)
29. S.A. Solopan, A.G. Belous, O.I. V'yunov, L.L. Kovalenko, Russ. J. Inorg. Chem. **53**, 157 (2008)
30. M. Bao, W. Li, P. Zhu, J. Mater. Sci. **28**, 6617 (1993)
31. D. Ghanbari, M. Salavati-Niasari, S. Karimzadeh, S. Gholamrezaei, J. NanoStruct. **4**, 227 (2014)
32. G. Nabiyouni, S. Sharifi, D. Ghanbari, M. Salavati-Niasari, J. NanoStruct. **4**, 317 (2014)
33. M. Panahi-Kalamuei, M. Mousavi-Kamazani, M. Salavati-Niasari, J. NanoStruct. **4**, 459 (2014)
34. F. Beshkar, M. Salavati-Niasari, J. NanoStruct. **5**, 17 (2015)
35. M. Goudarzi, D. Ghanbari, M. Salavati-Niasari, J. NanoStruct. **5**, 110 (2015)
36. S. Moshtaghi, M. Salavati-Niasari, D. Ghanbari, Summer J. NanoStruct. **5**, 169 (2015)